Reaction Kinetics, Mechanisms and Catalysis (2022) 135:1651–1664
https://doi.org/10.1007/s11144-022-02200-2

Photocatalytic oxidative degradation of methyl orange by a novel g-C_3N_4@ZnO based on graphene oxide composites with ternary heterojunction construction

Chunling Lin[1] · JinCang Su[1] · Zhengyang Chen[2] · SiYu Zhang[3] · Qinlong Gong[1] · Yaokang Qu[1] · Jiangdong Fei[1] · Xiang Ye[1] · Jiaoxia Zhang[2]

Received: 3 January 2022 / Accepted: 14 March 2022 / Published online: 21 March 2022

Abstract

Photocatalyst composites of g-C_3N_4/ZnO/GO (graphene oxide) were successfully prepared by sol–gel method combined with thermal polycondensation. The composites were characterized by SEM, XRD, TGA, FT-IR, UV–vis and physical adsorption. The electrical properties of g-C_3N_4/ZnO/GO composites were characterized by open circuit potential method and AC impedance method. The degradation of methyl orange by composites was studied. The results demonstrate that composites have better photocatalytic efficiency for the degradation of methyl orange than g-C_3N_4. The most efficient photocatalytic degradation of methyl orange stimulated wastewater adopt that 1 g/L of composites solution, 120 min and degradation time at 35 °C with adding 120 mL/L of H_2O_2.

Keywords Graphite-like carbon nitride · Ternary composites · Hydrothermal synthesis · Photocatalytic oxidative degradation · Methyl orange

Introduction

With the development of modern industrialization, contamination of water resources is getting worse and worse. But human requirement becomes higher and higher for the healthy environment. The increasing attention has been paid to the water treatment especially for organic dyes. Nitrogen-containing dyes pose a serious threat to

✉ Chunling Lin
chunling405@xsyu.edu.cn

[1] School of Chemistry and Chemical Engineering, Xi'an Shiyou University, Xi'an 710065, Shaanxi, China

[2] School of Materials Science and Engineering, Jiangsu University of Science and Technology, Zhenjiang 212003, Jiangsu, China

[3] School of Materials Science & Engineering, Shandong University, Jinan 250061, Shandong, China

human and other organisms in recent years. The adsorption technique among all of the removal methods is the most perhaps adopted method due to the low cost and convenience. Nanomaterials show higher adsorption efficient than the corresponding bulk materials owing to the nano-sized effects [1, 2].

In recent years, degradation of pollutant effluents by green technologies becomes significantly attractive research topic. Since sunlight may be a renewable natural energy, more and more scholars are curious about the treatment processes utilizing the solar energy [3–5]. A photocatalyst means the materials are activated by absorbing a photon and is capable of accelerating a reaction without being consumed [6]. Hence, semiconductor photocatalysis has become one of the most promising technologies due to its ability to utilize sustainable solar energy for the treatment of pollutant effluents without causing any side effects to the environment.

So far, a large number of semiconductor materials such as TiO_2 [7–10], ZnO [11, 12], WO_3 [13, 14], CdS [15], ZnS [16] have been explored as active photocatalysts for photodegradation of pollutants. Among these semiconductor materials, TiO_2 has emerged as the most common semiconductor since Fujishima and Honda reported photoelectrochemical water splitting in 1972 [17]. For decades, TiO_2 has emerged as the most common researched semiconductor several organic pollutant degradation resulting from its photocatalytic properties, hydrophilicity, high reactivity, non-toxicity, chemical stability, and low costs [18–20]. Due to its large band energy, TiO_2 can only absorb solar energy in the UV regions which only constitutes 4% of the total solar energy irradiated [21].

Recently, graphitic carbon nitride (g-C_3N_4) without metal composite became the highlight due to its narrow band gap of 2.7 eV which permits it to absorb visible light directly without any modification [22]. Graphitic carbon nitride exhibits high thermal and chemical stability, owing to its tri-striazine ring structure and high condensation [23]. Although various graphitic carbon nitride semiconductors have been studied for photocatalytic degradation of pollutants, their photocatalytic performance remains unsatisfactory suffering highly from charge (electron-holes) recombination [24]. Hence, researchers have been devoted to expanding the range of light absorption and enhancing the separation effect of photogenic carriers [25, 26]. To overcome the electron–hole recombination in a single g-C_3N_4 semiconductor, different measures have made toward developing novel photocatalytic systems with high photocatalytic activities, including metal [27–30] or non-metal doping [31, 32] and coupling with other semiconductor materials [33, 34]. Among these methods, heterostructure graphitic carbon nitride photocatalysts semiconductors has proven to be potential for use in enhancing the efficiency of photocatalytic pollutant degradation through the promotion of the separation of photogenerated electron–hole pairs and maximizing the redox potential of the photocatalytic system [35–42].

ZnO has been discovered very early and has been used in nanomaterial engineering [43], coatings [44], biological [45] and medical [46] The low energy valence band of ZnO is full of electrons, while the second high energy valence band has no electrons. Therefore, when ZnO is irradiated with light, photo-generated electron–hole pairs are generated [44], which paves the way for its outstanding performance in the field of photocatalytic degradation. Graphene is a two-dimensional allotrope of crystalline carbon formed by hexagonally arranging sp2-bonded carbon

atoms, which presents excellent optical properties, transparency, mechanical flexibility, and good thermal and chemical stability [47]. Graphene oxide (GO), an oxidized derivative of graphene, is a promising carbon material that has attracted significant interest over the last decade [46]. A large of functional groups on its basal planes such as hydroxyl and epoxy groups, in addition to carbonyl and carboxyl groups located at the sheet edges, are formed [47]. In order to take full advantage of the above three materials, in this study, g-C_3N_4/ZnO/GO composites were prepared to explore their photocatalytic efficiency for the degradation of methyl orange.

Materials and experiment

Materials

Methyl orange was purchased from Chengdu Kelong Chemical Reagent Factory and was used without further purification. Melamine ($C_3H_6N_6$, AR grade) as a precursor of g-C_3N_4 was obtained from Shanghai Macklin Biochemical Co. Ltd. $Zn(Ac)_2$ (AR grade) was obtained from Tianjin Fuchen Chemical Reagent Factory. Oxide graphene was supplied from Shanghai McLean Biochemical Technology Co. Ltd. Sodium hydroxide (NaOH, AR grade), was purchased from Tianjin Tianli Chemical Reagent Co. Ltd, H_2O_2 (30%) was obtain from Tianjin Kemiou Chemical Reagent Co. Ltd, Ethyl alcohol (95%, AR grade) was purchased from Tianjin Lianlongbohua Pharmaceutical Chemistry Co. Ltd.

Experimental method

Preparation of the g-C_3N_4/ZnO/GO composites

Soft templated synthesis of g-C_3N_4 The g-C_3N_4 was synthesized by heating melamine powder. Five grams of melamine powder and ammonium fluoride at the mass ratio of (1:1) were put into a crucible, and then heated at 520 °C in a muffle furnace for 4 h. After cooling to room temperature, the yellow product was dried by oven, collected and milled into a powder for further use. A certain amount of g-C_3N_4 powder was added into deionized water and ultrasonic dispersed for another 1 h.

Preparation of ZnO/g-C_3N_4/GO 50 mL $Zn(Ac)_2$ (5 wt%) was added to the solution with vigorous agitation at ambient temperature to obtain a light yellow suspensions. Sodium hydroxide solution 30 mL (1 M NaOH) was added to the suspensions drop by drop to avoid excessive local precipitation while stirring. The suspension was transferred into a 100 mL single flask, stirred for 1 h with water bath at 80 °C, 30 mL GO 1 (g/L)suspension was ultrasonic dispersed for 0.5 h, and 0.1 mL (about two drops) ammonium oxide of nonylphenol polyether was added into the GO suspension. The suspension was added rapidly into the dispersion to stir for 2 h by water bath. Then, the mixture, which included 10 ml g-C_3N_4 (5 wt%) suspension dispersing by ultrasound for 0.5 h,was put into hydrothermal reactor was added at 180 °C for 5 h. At last,

the product was filtrated and washed several times with deionized water and dried at 110 °C for 3 h to obtain composites of g-C_3N_4/ZnO/GO. Fig. 1 shows the preparation schematic diagram of composites.

Photocatalytic degradation of methyl orange by catalyst

0.05 g composites of g-C_3N_4/ZnO/GO was added to 100 mL volumetric flask containing 50 mL 10 mg/L MO stimulated waste water, and ultrasonic dispersion was performed for 30 min in dark conditions. The suspension was then irradiated with stimulated sunlight. 5 mL of the suspension was sampled every hour, centrifuged, and the supernatant was taken for visible spectrophotometer test. Since the solution of methyl orange was unstable, the absorbance of methyl orange without catalyst was measured under the same conditions as the control,

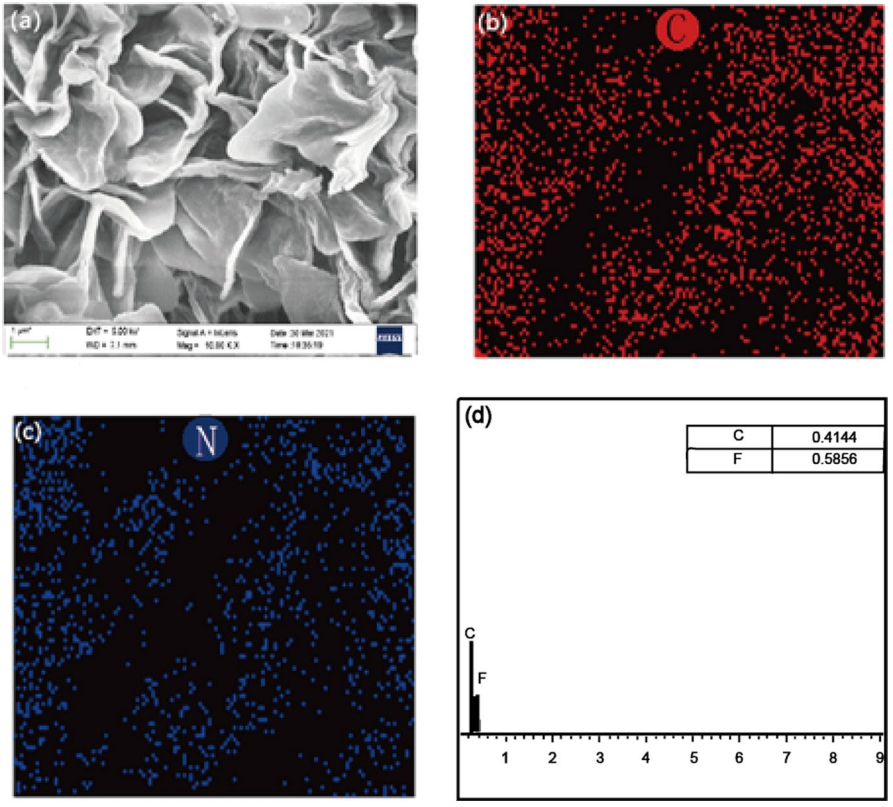

Fig. 1 SEM of g-C_3N_4 (**a**) and g-C_3N_4/ZnO/GO (**e**), mapping of g-C_3N_4 (**b, c**) and g-C_3N_4/ZnO/GO (**f, g, h**), EDS of g-C_3N_4 (**d**) and g-C_3N_4/ZnO/GO (**i**) composite materials (Putting the sample into the gold spraying instrument, and then take it into the scanning area of nitrogen atmosphere. The selected samples were scanned. Acceleration voltage: 0.2–30 kV; magnification: 5–30,000 times; probe current: 0.5 Pa^{-5} μA)

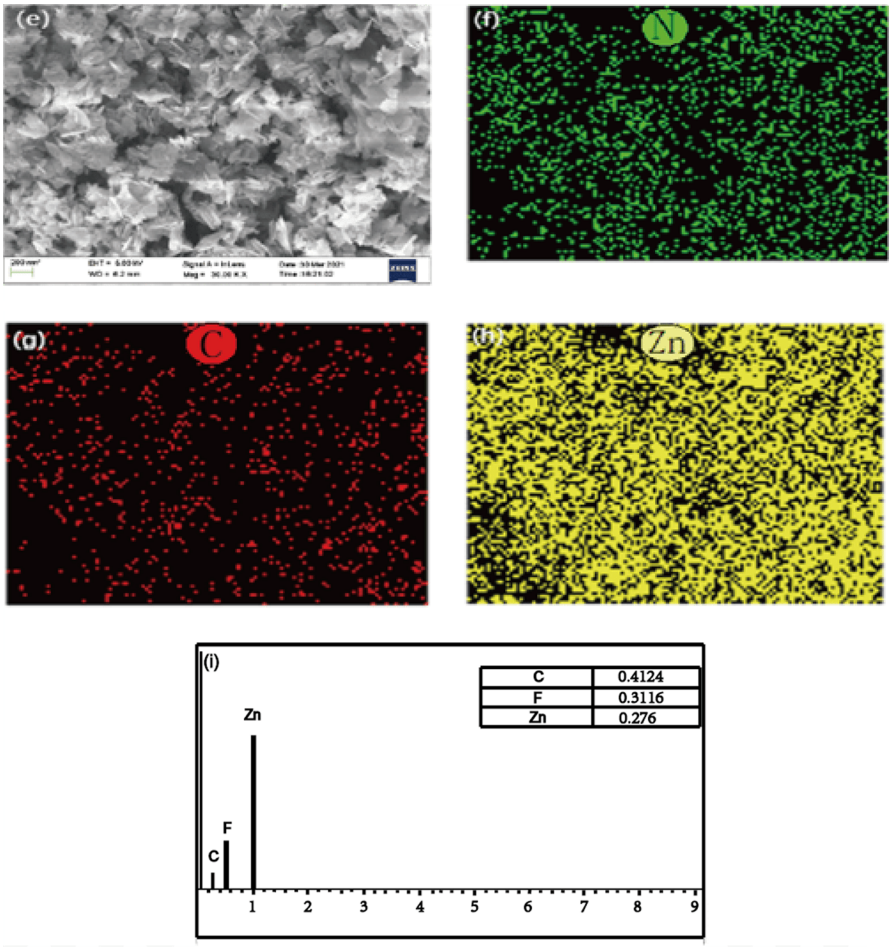

Fig. 1 (continued)

and the degradation ratio was calculated based on this. According to the absorbance, MO degradation ratio was calculated by the following formula.

$$R = \frac{A_t - A_0}{A_0} \times 100\%,$$

where R is the degradation ratio of MO. A_0 and A_t are the absorbance strength of the solution at initial time and time of t.

The concentration of methyl orange solution degraded by photocatalytic material was determined by spectrophotometry, and the standard curve of solution was showed in Fig. 1S.

Characterization

The crystalline phase of composites was tested by X-ray diffractometer (XRD-6000, Shimadzu, Japan) scanning from 10° to 90°. The morphology of g-C_3N_4 was observed by scanning electron microscopy (SEM, LEO1530, Leo Electron Microscopy Co. Ltd., Germany). Thermalgravimetric analyzer (TGA-DSC 1, METTLER TOLEDO, Germany) was conducted at a temperature range of 25–800 °C and a heating rate of 20 °C/min to test the samples' heat stability in a nitrogen atmosphere. Nicolet 5700 Fourier Transform infrared spectrometer (FTIR-5700, Thermo Electron Corporation) was recorded with the wavenumber range at 400–4000 cm^{-1}. The solid sample (1–2 mg) was pressed into a transparent sheet together with KBr. The photocatalytic properties were tested by ultraviolet spectrophotometer (UV–vis-2600, Shimadzu Analytical Instruments Corporation, Japan) and the wavelength range is 185–800 nm. Raman spectrometer (RL, Renishaw 1000) was tested with an excitation wavelength of 0–1000 nm Slit100 micron, Hole400, exposure time 20 s, three cycles. The specific surface of sample, the distribution of pore area to pore volume and the total pore volume were performed by physical adsorption method (ASAP-2020, Mcmerritt Instrument Co., Ltd.). The electrical properties of composites were characterized by open circuit potential method and AC impedance method using electrochemical workstation (CS350a, Wuhan Cost Co. Ltd., China). The photoluminescence (PL) spectra of the samples was measured by the Lumina fluorescent photometer (Lumina, Thermo Fisher Instrument Co. Ltd., USA) at the wavelength range: EX 190–900 nm, EM: 190–900 nm.

Results and discussion

The morphology of the prepared material was investigated by SEM. As can be seen from Fig. 1, compared with Fig. 1a and e, Obviously, g-C_3N_4 has a layered structure (Fig. 1a). The g-C_3N_4/ZnO/GO has a significantly decrease in size than g-C_3N_4 (Fig. 1e), and the ZnO and GO are successfully loaded on the g-C_3N_4, which will increase the surface area and heterojunction of the material and is more conducive to photoelectron transfer. The elemental mapping images which determined the elemental composition of C, N in C_3N_4 with different colors are shown in Fig. 1b and c. Further, C and N elements of g-C_3N_4 in Fig. 1d and f–i shows that C and N element is uniformly formed in the composites and zinc ions are uniformly distributed in the composites.

Fig. 2S shows the XRD patterns of photocatalytic samples. For Fig. 2Sa, a weak diffractive peak of g-C_3N_4 (100) lattice plane is at 13.1°, which induced by stacking in planar elements. While the second diffraction peak pair of g-C_3N_4 corresponds to the (200) lattice plane of g-C_3N_4 at 27.5°, which comes from inter-lamellar stacking of the conjugated aromatic system, that confirms the graphite-like lamellar structure of g-C_3N_4. For the g-C_3N_4/ZnO/GO composites, the plot shows strong and sharp diffraction peaks at 30–80°. The diffraction angle of ZnO is $2\theta = 31.77°$, 36.25°, 47.53°, 56.60°, 62.86°, 66.38°, 72.56°, 76.95° corresponding to (100), (101), (102), (110), (103), (200), (004), (202) lattice planes of hexagonal phase ZnO. However,

no significant characteristic diffraction peaks of g-C_3N_4 were observed in photocatalysts composites because the diffraction peaks of zinc oxide were too strong to override the g-C_3N_4.

The thermal stabilities of photocatalysts composites are showed in Fig. 2Sb according to the TGA curves. In the first stage of g-C_3N_4, a weight loss of about 5% is observed at temperatures of 100–250 °C, which is related to the evaporation of water/solvent which was absorbed into the pores of the structure. The g-C_3N_4 shows a sharp weight loss from 400 to 726 °C, which is attributed to the thermal decomposition of 3-s-triazine unit deamination polycondensation. For the g-C_3N_4/ZnO/GO composites, a weight loss of about 5% is observed at temperatures of 100–260 °C, which is also related to the evaporation of water/solvent that was absorbed into the pores of the structure. The weight loss between 260 and 400 °C result from the aerobic decomposition of oxygen-containing groups in GO releases CO, CO_2 and H_2O. The total weight loss of g-C_3N_4/ZnO/GO composites is only 25% of the original weight that is obviously higher than g-C_3N_4. Therefore, the thermal stability of g-C_3N_4/ZnO/GO composites is greatly improved compared to g-C_3N_4 due to the incorporated ZnO and GO.

Fig. 2Sc shows the FTIR of g-C_3N_4/ZnO/GO composites and g-C_3N_4. The g-C_3N_4 spectrum has strong absorption peaks at 1254, 1342, 1389, and 1612 cm^{-1} corresponding to the C–N and C=N stretching vibrations on the carbon–nitrogen ring. The absorption peak at 839 cm^{-1} corresponds to the backbone of the triazine ring vibrates. The broad absorption peaks at 3100 to 3400 cm^{-1} corresponding to the -OH peaks. It is also likely to be caused by –NH and $–NH_2$ residues [25] at the defect position of the aromatic ring. g-C_3N_4/ZnO/GO composites and g-C_3N_4 basically have the similar peaks, but the carbon and nitrogen characteristic peaks at 1254 and 1612 cm^{-1} are slightly weakened, which indicates that g-C_3N_4, ZnO, and GO are not simple physical mixing, but forming a heterojunction structure.

Fig. 2Sd shows the UV–visible absorption spectra of g-C_3N_4/ZnO/GO composites and g-C_3N_4. It can be seen from Fig. 2Sd that the maximum absorption intensity of g-C_3N_4 is at 280 nm, while the g-C_3N_4/ZnO composites is at 372 nm, it indicates that the maximum absorption wavelength of the composite materials have obvious red shift, because of the formation of a heterostructure between g-C_3N_4, ZnO and GO, which is more conducive to the absorption of visible light, and the photocatalytic effect will better than the g-C_3N_4.

Raman spectroscopy was used to study the ordered/ disordered crystal structures of carbonaceous materials. Thus, we utilized it to examine the changes that occurred in the structure of the graphene nanomeshes as compared to the as-prepared GO sheets, as shown in Fig. 2Se. The well-known characteristics of carbon materials in Raman spectra are the G band (1580 cm^{-1}), which is generally assigned to the E_{2g} phonon of sp^2 bonds of carbon atoms, and the D band (1350 cm^{-1}) as a breathing mode of point phonons of A_{1g} symmetry, which is attributed to local defects and disorders, particularly the defects located at the edges of graphene and graphite platelets [42]. Hence, the smaller ID/IG peak intensity ratio of a Raman spectrum can indicate lower defects and disorders of the graphitized structures containing the disorders caused at the edges of the carbon platelets. The Raman spectra shown in Fig. 2Se display the D and G bands at about 1182 and 1442.5 cm^{-1}, respectively. It

was also found that the ID/IG ratio increased from 1.00 for the GO sheets to 0.9404 for the graphene nanomeshes. This decrease was assigned to unformation of the pores in the graphene sheets. By increasing the graphene nanomeshes by hydrazine, the ID/IG ratio decreased to 1.18, which can be assigned to more graphitization of the nanomeshes due the reduction process in composites of g-C_3N_4/ZnO/GO. Raman spectroscopy is also utilized to investigate the single-, bi-, and multilayer characteristics of graphene and GO layers. For instance, it was shown that the G band of the single-layer graphene, located at 1585 cm^{-1}, shifts about 143 cm^{-1} into lower wavenumbers after stacking 2–6 graphene layers. Moreover, the shape and position of the 2D band are known as key parameters to judge both formation and the layer numbers of the grapheme sheets [46].

As shown in Table 1, the BET specific surface area, BJH adsorption specific surface area, and BJH desorption specific surface area of g-C_3N_4/ZnO/GO composites are 46.4541 m^2/g, which are twice that of g-C_3N_4. BJH adsorption specific surface area, and BJH desorption specific surface area of g-C_3N_4/ZnO/GO composites are 271.4238 and 36.4541 m^2/g, which are nearly three times that of g-C_3N_4. As shown in Fig. 4Sc, the pore volume of g-C_3N_4/ZnO/GO composites is also much larger than that of g-C_3N_4. After ternary recombination, the pore volume further increases. The increase of specific surface area and pore volume is not only helpful to increase the adsorption amount of pollutants, but also to improve the transfer and diffusion of photoelectrons in the composite material to promote the photocatalytic oxidation efficiency. Compared with g-C_3N_4, the average BET pore size, average BJH pore size, and average BJH desorption pore size of g-C_3N_4/ZnO/GO composites has tripled. This shows that loading of ZnO and GO is beneficial to increase the pore volume. GO has a two-dimensional single-layer honeycomb structure, and it is not easy to block the original holes of g-C_3N_4. Or it can be form a larger hole in space, which lead to increasing hole capacity. Fig. 3Sa and 3Sb are the N_2 adsorption and desorption isotherms of g-C_3N_4 and g-C_3N_4/ZnO/GO composites, respectively.

Table 1 Physical adsorption properties of g-C_3N_4 and g-C_3N_4/ZnO/GO composite materials

Physical index	g-C_3N_4	g-C_3N_4/ZnO/GO
BET specific surface (m^2/g)	11.7634	33.0396
BET average adsorption pore size (nm)	242.5208	271.4238
BJH adsorption specific surface area (m^2/g)	12.612	34.109
BJH desorption specific surface area (m^2/g)	15.3042	36.4541
BJH adsorption pore volume (cm^3/g)	0.0709	0.2212
BJH desorption pore volume (cm^3/g)	0.0708	0.2216
BJH average adsorption pore size (nm)	225.095	259.439
BJH mean desorption pore size (nm)	185.261	243.172
Total pore volume (cm^3/g)	0.0713	0.2242

Weight 0.2 g sample, set degassing temperature at 300 °C, heating rate at 10 °C/min, degassing for 6 h, analysis for 5 h. The specific surface area, pore area versus pore size distribution and total pore volume were determined. Temperature range: 40–450 °C; specific surface area: 0.0005 m^2/g; pore size analysis range: 3.5 Å–5000 Å, micropore section resolution: 0.2 Å

The desorption isotherms of g-C_3N_4, g-C_3N_4/ZnO/GO composites are all above the adsorption isotherm with H_3 hysteresis loop which is hysteresis loops at 0.44–1.0 of P/P0 which is helpful to adsorb pollutants and improve the transfer and diffusion of photoelectrons in the composite material to promote the photocatalytic oxidation efficiency.

Fig. 4Sa shows the open-circuit potential of composites. It can be seen from Fig. 4Sa that the conductivity of g-C_3N_4/ZnO/GO composites is better than that of g-C_3N_4 that means the composites have better transfer electron properties. Fig. 4Sb shows g-C_3N_4/ZnO/GO composites and g-C_3N_4 of AC impedance map (EIS). Generally, the small radius of the semicircle indicates the rapid separation and transfer of photogenerated carriers. The greater the diameter of the semicircle, the more difficult of the electron transfer. The composite material has the smallest resistance (Fig. 4Sb), which indicate it is easier to transfer electron and high photocatalytic rate.

Photoluminescence measurement was regarded as a useful tool to detect the possibility of recombination process for photo-generated charge carriers. The electron–hole recombination rate depends on the emission intensity. A high PL emission intensity indicates the severe electron–hole recombination rate. As shown in Fig. 4Sc, the g-C_3N_4/ZnO/GO composites exhibited a strong emission peak due to its high electron–hole recombination rate, which is mainly due to the effective electron transfer between two components. the PL emission intensity of g-C_3N_4 is greatly decreased. Apparently, the formation of heterojunction between g-C_3N_4, ZnO and GO takes positive effects on the separation and transfer of photogenerated charge carriers, facilitating photocatalytic activity for O_2 generation and MO degradation.

The g-C_3N_4/ZnO/GO composites as the sorbents was used to treat the MO stimulated waste water. the concentration of g-C_3N_4/ZnO/GO composites, temperature and time of adsorption on the removal ratio were discussed. The concentration of g-C_3N_4/ZnO/GO composites is considered as variate from 0.1 to 1.00 g/L with the constant of 25 °C, 40 min and 10 mg/L of MO for the adsorption process (see Fig. 5Sa). With the concentration increasing of g-C_3N_4/ZnO/GO composites, the removal ratios also are evidently improved because the more g-C_3N_4/ZnO/GO composites bring the larger adsorption surface area to promote the faster electron transfer and obtain greater adsorption capacity. But removal ratio holds around the 91.4% when the concentrations continually increase after 1.00 g/L which imply the adsorption and desorption performance of MO stimulated waste water reach to the activated balance for the g-C_3N_4/ZnO/GO composites adsorbent. So, the g-C_3N_4/ZnO/GO composites 1.00 g/L is taken as the best content for the 10 mg/L of the MO in water considering the cost and removal efficiency.

About the treating time from Fig. 5Sb, the removal ratio of the MO stimulated waste water gradually increases with the prolonging treating time. However, when the adsorption time reaches 120 min, the removal ratio MO of stimulated pollutant effluents reaches up to 91.2% and become stable after 120 min adsorption time.

Finally, the temperature is considered as variate from 25 to 45 °C with the constant of 1 g/L of g-C_3N_4/ZnO/GO composites, 120 min, and 10 mg/L of the MO solution for the adsorption process to determine the removal ratio for MO in water (see Fig. 5Sc). With the increasing temperature (up to 35 °C), the removal ratios

of g-C_3N_4/ZnO/GO composites, also are gradually increasing to around 91.2% from 25 to 35 °C. The reason is that the adsorption rate of methyl orange waste water become fast resulting in the fast degradation rate of the composite with the increasing of temperature. However, when the adsorption reaches equilibrium, the adsorption rate will not increase when the temperature is increased. the degradation of methyl orange by composites of g-C_3N_4/ZnO/GO was under simulated sunlight and the shadows respectively, the results was as shown in Fig. 5Sd, the rate of degradation of methyl orange in the shadows was no more than 52%, But the degradation rate of methyl orange in simulated sunlight is more than 92%, including the same concentration of the composite material, the same degradation time and the same degradation temperature, It was evidence that the degradation of MO by composites of g-C_3N_4/ZnO/GO was photocatalytic degradation.

Then, the used sample is filtered and dried, and then the photocatalysis experiment is carried out again to evaluate the reproducibility of g-C_3N_4 and g-C_3N_4/ZnO/GO composites with the sample solution of 1 g/L at 35 °C (see Fig. 6S). The five curves were found to be close and almost identical, and the maximum removal rate is unchanged. The removal rate can still reach 90.1% even after five times of re-use, indicating the high reproducibility of the photocatalyst.

At last, in order to explore the main active species of g-C_3N_4/ZnO/GO compositesin photo catalytical reactions, the benzoquinone, isopropanol oxalate, EDTA disodium salt as trapping agents were used to capture $OH^{\cdot}$, $O^{2-\cdot}$ and (h^+). As shown in Fig. 7S, the removal rate of MO stimulated waste water by adding benzoquinone is almost 0, which means that benzoquinone captured $O^{2-\cdot}$. However, the addition of EDTA disodium salts and isopropanol has little effect on the photocatalytic activity of g-C_3N_4/ZnO/GO composites, which indicates that $O^{2-\cdot}$ is the main active species in the photocatalytic removal of MO by C_3N_4/ZnO/GO composites.

Based on the above experiment results, the mechanism of the photocatalytic reaction in the system g-C_3N_4/ZnO/GO composites is proposed as illustrated. Due to the rapid recombination of electron-hole pairs, the catalytic efficiency of g-C_3N_4 is very low. After the ZnO and GO composite is loaded onto the surface of g-C_3N_4 to provide more hydrogen evolution active sites and accelerates electron transform, thereby enhancing the activity of the g-C_3N_4/ZnO/GO composites catalyst. In detail, heterogeneous under stimulated visible light irradiation absorb the energy of the photon and are excited to generate photo-generated electron-hole pairs. The large specific surface area heterogeneous g-C_3N_4/ZnO/GO composites have a stronger absorption rate of visible light, thereby generating more photo-generated carriers.

g-C_3N_4/ZnO/GO composites photocatalytic degradation mechanism was discussed as follows. Under visible light irradiation, g-C_3N_4 is excited to form photo-generated electron-holes; since the CB (conduction band) of g-C_3N_4 is − 1.27 eV [48], the CB of ZnO is − 0.505 eV. Therefore, the photogenerated e^- is transferred from the conduction band of g-C_3N_4 to ZnO; and the excellent conductivity of GO can accelerate the electron transfer. These e^- are further adsorbed with O_2 on the surface of the catalyst to form an active center $^{\cdot}O_2^-$ at the same time, the holes formed on the valence band of g-C_3N_4 are combined with H_2O to form $^{\cdot}OH$. These highly reactive free radicals can eventually degrade MO into small molecules such as H_2O and CO_2. Because g-C_3N_4, ZnO and GO

form a heterojunction, it prevents photo-generated electron–hole recombination and improves photocatalytic activity. The above process can be described by the following formula:

$$e^- + O_2 \rightarrow O^{-2} \tag{2}$$

$$O^{-2} + e^- + 2H^+ \rightarrow H_2O_2 \tag{3}$$

$$H_2O_2 + e^- \rightarrow OH + OH^- \tag{4}$$

$$h^+ + H_2O \rightarrow OH + H^+ \tag{5}$$

$$\bullet OH + MB \rightarrow CO_2 + H_2O \tag{6}$$

Hydrogen peroxide (H_2O_2) provides enough oxygen to form more free radicals and increases the concentration of free radicals in the case of ultrasound. When the H_2O_2 were added into methyl orange simulated waste water, it can be seen from Fig. 8S, the removal of methyl orange simulated wastewater increases firstly and then tends to be stable with the increase of the amount of H_2O_2. But excessive H_2O_2 will inhibit the generation of hydroxyl radical in the case of excessive H_2O_2. The contact volume of H_2O_2 is 120 mL/L.

Conclusion

In this paper, g-C_3N_4/ZnO/GO composite materials were synthesized. The synthesized g-C_3N_4/ZnO/GO composite shows good efficiency in the removal of MO stimulated waste water. The removal mechanism of MO with g-C_3N_4/ZnO/GO composite materials is controlled by electrostatic interactions, hydrogen bonding, ternary heterojunction construction, The photocatalytic degradation of methyl orange reaches the best effects with 120 min of illumination at is 35 °C by 1 g/L of g-C_3N_4/ZnO/GO added 120 mL/L of H_2O_2. The multi-electron structure of fluorine in ammonium fluoride in soft template method may be beneficial to photoelectron transfer.

The formation of g-C_3N_4/ZnO/GO heterojunction reduces the recombination rate of photo-generated electrons and holes, and can form more highly active free radicals, thereby improving the catalytic efficiency.

Supplementary Information The online version contains supplementary material available at https://doi.org/10.1007/s11144-022-02200-2.

Acknowledgements We gratefully acknowledge the supports from the Special fund of Shaanxi Provincial Education Department (16JK1612), the Open Project of Zhenjiang Key Laboratory of Marine Functional Thin Film Materials High Technology Research (ZHZ2019008), Key Research and Development Project of Shaanxi Province (2017GY-180) and Provincial College Students Innovation and Entrepreneurship Program (S202010705115).

References

1. Wang J, Tang L, Zeng G, Deng Y, Liu Y, Wang L, Zhou Y, Guo Z, Wang J, Zhang C (2017) Atomic scale g-C_3N_4/$Bi_2WO_6$2D/2D heterojunction with enhanced photocatalytic degradation of ibuprofen under visible light irradiation. Appl Catal B Environ 209:285–294
2. Gao Y, Zhang J, Zhang Z, Li Z, Xiong Q, Deng L, Zhou Q, Meng L, Du Y, Zuo T, Yu Y, Lan Z, Gao P (2021) Plasmon-enhanced perovskite solar cells with efficiency beyond 21%: the asynchronous synergistic effect of water and gold nanorods. ChemPlusChem 86(2):291–297
3. Liu S, Hu Q, Qiu J, Wang F, Lin W, Zhu F, Wei C, Zhou N, Ouyang G (2017) Enhanced photocatalytic degradation of environmental pollutants under visible irradiation by a composite coating. Environ Sci Technol 51(9):5137–5145
4. Rasheed T, Bilal M, Li C, Nabeel F, Khalid M, Iqbal H (2018) Biology catalytic potential of biosynthesized silver nanoparticles using *Convolvulus arvensis* extract for the degradation of environmental pollutants. J Photochem Photobiol B 181:44–52
5. Liu J, Ke J, Li D, Sun H, Liang P, Duan X, Tian W, Tadé MO, Liu S, Wang S (2017) Interfaces oxygen vacancies in shape controlled Cu_2O/reduced graphene oxide/In_2O_3 hybrid for promoted photocatalytic water oxidation and degradation of environmental pollutants. ACS Appl Mater Interfaces 9(13):11678–11688
6. Lin C, Liu B, Pu L, Sun Y, Xue Y, Chang M, Li X, Lu X, Chen R, Zhang J (2021) Photocatalytic oxidation removal of fluoride ion in wastewater by g-C_3N_4/TiO_2 under simulated visible light. Adv Compos Hybrid Mater 4(2):339–349
7. Akhavan O, Ghaderi E (2009) Photocatalytic reduction of graphene oxide nanosheets on TiO_2 thin film for photoinactivation of bacteria in solar light irradiation. J Phys Chem C 113:20214–20220
8. Thompson TL, Yates JT (2006) Surface science studies of the photoactivation of TiO_2 new photochemical processes. Chem Rev 106(10):4428–4453
9. Du X, Bai X, Xu L, Yang L (2020) Visible-light activation of persulfate by TiO_2/g-C_3N_4 photocatalyst toward efficient degradation of micropollutants. Chem Eng J 384:123–245
10. Chunling CL, Yifeng G, Jiaoxia Z, Dan X, Hua F, Jiayong T, Chunli Z, Chanjuan Z, Yuqing L, Honggang L (2020) GO/TiO_2 composites as a highly active photocatalyst for the degradation of methyl orange. J Mater Res 35(10):1307–1315
11. Tian C, Zhang Q, Wu A, Jiang M, Liang Z, Jiang B, Fu H (2012) Cost-effective large-scale synthesis of ZnO photocatalyst with excellent performance for dye photodegradation. Chem Commun (Camb) 48(23):2858–2860
12. Rokhsat E, Akhavan O (2016) Improving the photocatalytic activity of graphene oxide/ZnO nanorod films by UV irradiation. Appl Surf Sci 371:590–595
13. Akhavan O, Choobtashani M, Ghaderi E (2012) Protein degradation and RNA efflux of viruses photocatalyzed by graphene−tungsten oxide composite under visible light. J Phys Chem C 116:9653–9659
14. Cui L, Ding X, Wang Y, Shi H, Huang L, Zuo Y, Kang S (2017) Facile preparation of Z-scheme WO_3/g-C_3N_4 composite photocatalyst with enhanced photocatalytic performance under visible light. Appl Surf Sci 391(Part B):202–210
15. Ucun OK, Montazeri B, Alaton İA, Hanci TÖ (2010) Treatment of industrial contaminants with zero-valent iron- and zero-valent aluminiumactivated persulfate: a case study with 3,5-dichlorophenol and 2,4-dichloroaniline. Turk J Chem 45(2):269–281
16. Anandan S, Miyauchi M (2012) Improved photocatalytic efficiency of a WO3 system by an efficient visible-light induced hole transfer. Chem Commun (Camb) 48(36):4323–4325
17. Fujishima A, Honda K (1972) Electrochemical photolysis of water at a semiconductor electrode. Nature 238(5358):37–38
18. Zhang J-X, Yi J, Jiao Y-T, Li S-Y, Shi X-L, Sun K (2018) Preparation and application of water-soluble TiO_2-ionic liquids hybrid nanomaterials. J Inorg Mater 33(5):577–581
19. Ismael M (2020) Enhanced photocatalytic hydrogen production and degradation of organic pollutants from Fe(III) doped TiO_2 nanoparticles. J Environ Chem Eng 8(2):103676
20. Alam U, Fleisch M, Kretschmer I, Bahnemann D, Muneer MJ (2017) One-step hydrothermal synthesis of Bi-TiO_2 nanotube/graphene composites: an efficient photocatalyst for spectacular degradation of organic pollutants under visible light irradiation. Appl Catal B 218:758–769
21. Fu J, Yu J, Jiang C, Cheng BJ (2018) g-C_3N_4-based heterostructured photocatalysts. Adv Energy Mater 8(3):1701503

22. Yan S, Li Z, Zou ZJ (2009) Photodegradation performance of g-C_3N_4 fabricated by directly heating melamine. Langmuir 25(17):10397–10401
23. Cui Y, Ding Z, Liu P, Antonietti M, Fu X, Wang X (2012) Metal-free activation of H_2O_2 by g-C_3N_4 under visible light irradiation for the degradation of organic pollutants. Phys Chem Chem Phys 14(4):1455–1462
24. Che H, Che G, Dong H, Hu W, Hu H, Liu C, Li C (2018) Fabrication of Z-scheme Bi_3O_4Cl/g-C_3N_4 2D/2D heterojunctions with enhanced interfacial charge separation and photocatalytic degradation various organic pollutants activity. Appl Surf Sci 455:705–716
25. Yu Q, Lin X, Li X, Chen J (2020) Photocatalytic Stille cross-coupling on gold/g-C_3N_4 nano-heterojunction. Chem Res Chin Univ 36(6):1013–1016
26. Wang S, Zhan J, Chen K, Ali A, Zeng L, Zhao H, Hu W, Zhu L, Xu X (2020) Potassium-doped g-C_3N_4 achieving efficient visible-light-driven CO_2 reduction. ACS Sustain Chem Eng 8(22):8214–8222
27. Li C, Wang Y, Li C, Xu S, Hou X, Wu P (2019) Simultaneously broadened visible light absorption and boosted intersystem crossing in platinum-doped graphite carbon nitride for enhanced photosensitization. ACS Appl Mater Interfaces 11(23):20770–20777
28. Liu R, Yang W, He G, Zheng W, Li M, Tao W, Tian M (2020) Ag-modified g-C_3N_4 prepared by a one-step calcination method for enhanced catalytic efficiency and stability. ACS Omega 5(31):19615–19624
29. Xu J, Long K-Z, Wang Y, Xue B, Li Y-XJ (2015) Fast and facile preparation of metal-doped g-C_3N_4 composites for catalytic synthesis of dimethyl carbonate. Appl Catal A 496:1–8
30. Huang J, Li D, Li R, Zhang Q, Chen T, Liu H, Liu Y, Lv W, Liu GJ (2019) An efficient metal-free phosphorus and oxygen co-doped g-C_3N_4 photocatalyst with enhanced visible light photocatalytic activity for the degradation of fluoroquinolone antibiotics. Chem Eng J 374:242–253
31. Hu C, Hung WZ, Wang MS, Lu PJJ (2018) Phosphorus and sulfur codoped g-C_3N_4 as an efficient metal-free photocatalyst. Carbon 127:374–383
32. Sumathi M, Prakasam A, Anbarasan PM (2020) Fabrication of ultrathin nanosheets of graphitic carbon nitride heterojunction with spherical shaped Bi_2O_3 nanoparticles for high performance visible light photocatalyst. J Cluster Sci 31(1):277–286
33. Fathi E, Derakhshanfard F, Gharbani P, Ghazi-Tabatabaei Z (2020) Facile synthesis of MgO/C_3N_4 nanocomposite for removal of reactive orange 16 under visible light. J Inorg Organomet Polym Mater 30(6):2234–2240
34. Praus P, Lang J, Martaus A, Svoboda L, Matějka V, Kormunda M, Šihor M, Reli M, Kočí K (2019) Composites of $BiVO_4$ and g-C_3N_4: synthesis, properties and photocatalytic decomposition of azo dye AO7 and nitrous oxide. J Inorg Organomet Polym Mater 29(4):1219–1234
35. Jo W-K, Selvam NCS (2015) Enhanced visible light-driven photocatalytic performance of ZnO-g-C_3N_4 coupled with graphene oxide as a novel ternary nanocomposite. J Hazard Mater 229:462–470
36. Zhang J, Li J, Liu X (2021) Ternary nanocomposite ZnO–g-C3N4–GO for enhanced photocatalytic degradation of RhB. Opt Mater 119:111351
37. Liu Q, Zhang S, Li E, Zhang Y, Xia S (2019) Facile fabrication of Fe_2O_3/nitrogen deficient g-C_3N_{4-x} composite catalysts with enhanced photocatalytic performances. J Wuhan Univ Technol Mater Sci Ed 34(5):1018–1023
38. Shen J, Li Y, Zhao H, Pan K, Li X, Qu Y, Wang G, Wang D (2019) Modulating the photoelectrons of g-C_3N_4 via coupling $MgTi_2O_5$ as appropriate platform for visible-light-driven photocatalytic solar energy conversion. Nano Res 12(8):1931–1936
39. Zhao Z, Sun Y, Dong FJ (2015) Graphitic carbon nitride based nanocomposites: a review. Nanoscale 7(1):15–37
40. Gu X, Li C, Yuan S, Ma M, Qiang Y, Zhu J (2016) ZnO based heterojunctions and their application in environmental photocatalysis. Nanotechnology 27(40):402001
41. Mclaren A, Valdes-Solis T, Li G, Tsang SC (2016) Shape and size effects of ZnO nanocrystals on photocatalytic activity. J Am Chem Soc 131(35):12540–12541
42. Akhavan O (2010) Graphene nanomesh by ZnO nanorod. ACS Nano 4(7):4174–4180
43. Guo Y, Wang H, He C, Qiu L, Yang XC (2009) Uniform carbon-coated ZnO nanorods: microwave-assisted preparation, cytotoxicity, and photocatalytic activity. Langmuir 25(8):4678–4684
44. Nourmohammadi A, Rahighi R, Akhavan O, Moshfegh A (2014) Graphene oxide sheets involved in vertically aligned zinc oxide nanowires for visible light photoinactivation of bacteria. J Alloys Compd 612:380–385

45. Jiang J, Pi J, Cai J (2018) The advancing of zinc oxide nanoparticles for biomedical applications. Bioinorg Chem Appl. https://doi.org/10.1155/2018/1062562
46. Jiao Y, Zhang J, Liu S, Liang Y, Li S, Zhou H, Zhang JJ (2018) The graphene oxide ionic solvent-free nanofluids and their battery performances. Sci Adv Mater 10(12):1706–1713
47. Zhang J, Li P, Zhang Z, Wang X, Tang J, Liu H, Shao Q, Ding T, Umar A, Guo ZJ (2019) Solvent-free graphene liquids: promising candidates for lubricants without the base oil. J Colloid Interface Science 542:159–167